ELSEVIER

Friedel–Crafts alkylation properties of aluminosilica SBA-15 meso/macroporous monoliths and mesoporous powders ☆

J.J. Chiu,[a] D.J. Pine,[a,b] S.T. Bishop,[a] and B.F. Chmelka [a,*]

[a] *Department of Chemical Engineering, University of California, Santa Barbara, CA 93106, USA*
[b] *Materials Department, University of California, Santa Barbara, CA 93106, USA*

Abstract

The catalytic activities of SBA-15 aluminosilica meso/macroporous monoliths (Si/Al = 72) and mesoporous powders (Si/Al = 70) have been investigated using batch Friedel–Crafts alkylation of single-ring aromatic compounds, including toluene, ethylbenzene, cumene, and styrene, with benzyl alcohol. The toluene alkylation activities of the meso/macroporous monolith catalysts were compared with nanoporous zeolite Beta (Si/Al = 75, average particle size ~ 10 µm) and mesoporous SBA-15 aluminosilica (average particle size ~ 25 µm), as powders and pellets (0.5 cm thick × 1 cm diameter) to study the effects of framework crystallinity, particle size, pore size, and pore structure on the overall conversion. Apparent reaction rate coefficients were quantified based on a model for the alkylation of toluene with benzyl alcohol via two parallel reaction schemes to benzyl toluene. Moderate toluene alkylation rates ($\sim 10^{-4}$ s^{-1}) and high selectivities (> 90%) for benzyl toluene were observed for meso/macroporous aluminosilica SBA-15 monoliths, compared to the mesoporous SBA-15 and zeolite Beta powders, which displayed faster alkylation rates ($\sim 10^{-3}$ s^{-1}), though were less selective (79 and 59%, respectively). In pellet form, both the mesoporous SBA-15 and the zeolite Beta materials yielded lower rates of alkylation ($\sim 10^{-4}$ s^{-1}), due to slower internal diffusion of reactants and products within the smaller pellet macropores, compared to the meso/macroporous monoliths. Diffusive resistances to mass transfer were quantified by estimating Thiele moduli and effectiveness factors for the different catalysts, based on benzyl alcohol diffusivities measured by PFG NMR. The aluminosilica meso/macroporous SBA-15 monoliths deactivated more slowly, retaining 92% of their original activities after one use, compared to 75, 76, and 0.6% for SBA-15 powder, SBA-15 pellet, and zeolite Beta powder catalysts, respectively.
© 2003 Elsevier Inc. All rights reserved.

Keywords: Bimodal porosity; Mesoporous/macroporous monoliths; SBA-15; Solid acid catalysts; Friedel–Crafts alkylation

1. Introduction

Friedel–Crafts alkylations are industrially important reactions used to produce numerous aromatic compounds [1,2]. Such processes often rely on liquid acid catalysts, such as AlCl$_3$, HF, and BF$_3$ [1], however, the separation and handling of the acid waste present undesirable economic, environmental, as well as health and safety issues. Recently, much effort has been devoted to developing and investigating the feasibility of using solid acids, such as zeolites and mesoporous aluminosilicas, as new means to catalyze alkylation and other reactions [3,4].

Among some of the systems and reactions studied, aluminosilicate zeolite Beta, zeolite Y, MCM-22, MCM-41, and other nanoporous and mesoporous materials have been

shown to be active catalysts for alkylation of benzene or toluene [5–8]. The acidic properties of these solids generally arise from cationic Brønsted or Lewis acid sites that are associated with tetrahedrally coordinated aluminum species in the aluminosilica frameworks [3]. These porous materials have uniform pore channels and high surface areas, making them good candidates for catalysts. However, because they are usually in the form of fine powders with particle sizes of 1–15 µm, there can be practical drawbacks to their use in industrial processes, including separation and handling for liquid-phase reactions or large pressure drops for gas-phase reactions. Systems with such fine particles are, therefore, frequently combined with a binder and extruded in the form of macroscopic beads or pellets or deposited onto inert nonporous substrates as monolithic catalysts [9]. In these different macroscopic forms, however, diffusive resistances to mass transport can be important, particularly when large particles or monoliths, fast chemical reactions, and/or slowly

---

☆ Supplementary data for this article may be found on ScienceDirect.
* Corresponding author.

diffusing molecular species are present. Indeed, liquid-phase alkylation reactions can be limited by mass transfer in some commercial zeolite catalysts to occur in only a thin outer layer of the extruded catalyst pellets [10].

In principle, for a given reaction rate, diffusion resistances may often be mitigated by increasing the mean pore size or by decreasing the macroscopic particle size or monolith dimensions. However, these strategies tend to reduce the overall surface area per unit mass of catalyst or reintroduce separation or pressure drop difficulties. An alternative approach that overcomes these compromises is to design catalytic materials with pore sizes on two independently adjustable length scales, one in the micrometer range to enhance mass transport and the other in the nanometer range to maintain high surface area. Hierarchically structured porous materials such as these, comprised of an interconnected macroporous inorganic framework structure with mesoporous walls, are expected to be especially desirable for promoting catalytic reactions that involve large molecular species. Bimodal meso/macroporous siliceous materials have been prepared as monoliths [11,12], thin films [13], threads [14], particles with small domain sizes (~ 100 µm) [15], and fractal structures or aggregates [16,17]. However, the preparation of large (> 1 cm) self-supporting (mechanically stable) meso/macroporous aluminosilica monoliths has not been reported, nor have their catalytic properties been investigated.

Here, we report a new synthesis procedure for the preparation of meso/macroporous aluminosilicas that combines emulsion and block-copolymer templating to produce centimeter-size, mechanically stable monoliths with interconnected macropores whose walls are comprised of ordered mesopores. This is achieved by making an oil-in-water (O/W) emulsion, where the continuous phase consists of an aqueous amphiphilic block copolymer mesophase (hexagonal or cubic), in combination with a network-forming aluminosilica sol. The emulsion oil droplets have a characteristic size of several hundred nanometers, which establishes the macropore dimensions. The volume fraction of the oil droplets is made sufficiently high ($\sim 70\%$) so that the droplets are in contact, and the macropores which they template are interconnected. Polymerization of the silica and alumina precursor species yields a mesoscopically ordered aluminosilica/block copolymer mesophase in the aqueous interstices between the micrometer-size oil droplets. The lattice constant of the mesophase is approximately 10 nm, or about 30 times smaller than the emulsion oil droplets for a typical sample. Removal of the organic species, for example by calcination or solvent extraction, results in a bimodal distribution of pore sizes established by the dimensions of the hydrophobic block copolymer and oil droplet regions.

Using emulsion droplets [18] rather than more rigid structure-directing agents, such as polystyrene spheres [15,19], is a key feature of this technique. Because the emulsion drops are deformable, macroscopic samples are able to accommodate stresses that arise during gelation and shrinkage [18].

Samples made using rigid spheres, by contrast, tend to break into small pieces that are seldom larger than a few hundred micrometers [15,19]. In addition, emulsification conditions can be adjusted to produce droplets with different mean sizes which are typically in the micron range. Moreover, this can be done to a large extent independently of the self-assembling block copolymer species used to direct the structure of the mesopores. This allows direct and independent control of macro- and mesopore dimensions, so the final pore structures can be tailored to different diffusion and reaction conditions. Liquid-phase Friedel–Crafts alkylation reactions are used here to evaluate the catalytic properties of bimodal meso/macroporous aluminosilica SBA-15 monoliths for comparison with zeolite Beta and mesoporous SBA-15 catalysts.

2. Experimental

2.1. Catalyst syntheses and characterization

2.1.1. Meso/macroporous aluminosilica SBA-15 monoliths

Aluminosilica meso/macroporous monoliths were synthesized using emulsion and block-copolymer templating, in combination with sol–gel chemistry. First, a polydisperse oil-in-water emulsion was prepared by adding silicone oil (PDMS—poly(dimethylsiloxane), viscosity ~ 350 cP, Gelest Inc.) to a 40 wt% aqueous solution of nonylphenolethoxy 7 (C_9PhEO_7, Rhodia Inc.). PDMS droplets were gently stirred into the solution until they occupied 70% of the total volume. The droplet diameters in this polydisperse emulsion varied from a few to several hundred micrometers. Monodisperse emulsions were obtained by subjecting the emulsion to a uniform shear strain (for droplet breakup) using a cylindrical Couette cell with a uniform gap width of 100 µm [20]. Typical shear rates were $\sim 8000/s$. The resulting emulsions had average droplet diameters that could be varied and were typically from 0.1 to 5 µm with a polydispersity of 20% for this particular system. Larger droplet sizes could be obtained and controlled by varying the shear rate, the viscoelasticity (i.e., surfactant type and concentration, oil viscosity, etc.) of the polydisperse emulsions, or the gap width of the Couette cell [20].

Triblock copolymers of ethylene oxide (EO) and propylene oxide (PO), either $EO_{20}PO_{70}EO_{20}$ (Pluronic P123, BASF Corp.) or $EO_{106}PO_{70}EO_{106}$ (Pluronic F127, BASF Corp.), were used as mesostructure-directing agents in the continuous aqueous phase of the O/W emulsion. Hexagonal or cubic mesostructural ordering was produced in the aqueous regions, as estimated according to the corresponding block copolymer/water phase diagrams [21]. Following the method of Feng et al. [22,23], a mixture of tetramethylorthosilicate (TMOS, 99%, Fisher Acros), water, hydrochloric acid, and aluminum chloride hexahydrate (99%, Aldrich) in mass ratios of 1 g TMOS:0.7 g HCl/H_2O (pH ~ 2.0):x g $AlCl_3$ (where x depends on the Si/Al ratio

desired) was stirred vigorously to hydrolyze the silica and alumina species. Upon removal of the by-product methanol by evaporation under vacuum, 0.48 g block copolymer per 1.0 g TMOS was added to the hydrolyzed sol and mixed until completely dissolved. This concentrated aluminosilica-block copolymer sol was then mixed with the premade oil-in-water emulsion in approximately equal proportions by mass. Air bubbles formed during mechanical mixing of the sol and emulsion were removed by centrifugation. Alumina and silica species in the resultant block copolymer sol–gel emulsion were allowed to polymerize for 3 days, after which the mixture was hydrothermally treated at 100 °C overnight, and the oil and residual block copolymer species were subsequently removed by solvent extraction. The materials were then calcined at 500 °C in air for 6 h to produce the final meso/macroporous SBA-15 monoliths.

2.1.2. Mesoporous aluminosilica SBA-15 powders

Hexagonal mesostructured aluminosilica SBA-15 powders were synthesized under acidic conditions similar to procedures described in Refs. [22,23] for siliceous samples, but modified here by adding an aluminum source. Pluronic P123 block copolymer species were used as the mesostructure-directing agents. Alumina and silica precursors ($AlCl_3$ and TMOS, respectively) were added to aqueous HCl (pH ~ 2.0) and mixed vigorously until the TMOS was completely hydrolyzed. Following the removal (under vacuum) of methanol produced by the hydrolysis of TMOS, the viscous sol was mixed homogeneously with the P123 block copolymer. The final mixture consisted of hydrolyzed TMOS, $AlCl_3$, P123, HCl, and water in the following proportions: 1 g TMOS:0.48 g P123:0.68 g HCl/H_2O (pH ~ 2.0):x g $AlCl_3$, where x was adjusted to achieve the desired Si/Al ratio. Gelation and aging occurred under ambient conditions for 3 days, followed by hydrothermal treatment at 100 °C overnight, and subsequent drying and calcination in air at 500 °C for 6 h. Pelleted samples were formed by pressing the calcined particles under ~ 120 MPa pressure into approximately 0.5-cm-thick $\times$ 1-cm-diameter disks.

2.1.3. Nanoporous zeolite Beta

Commercially available nanoporous crystalline zeolite Beta powder (Si/Al = 75, Zeolyst International) was used as received for catalytic activity measurements of powder samples. Pelleted samples were formed by pressing the powder particles under ~ 120 MPa pressure into approximately 0.3-cm-thick $\times$ 1-cm-diameter disks, such that the pellet masses matched those of the SBA-15 pellets.

2.2. Catalyst characterization

Surface areas of the aluminosilica meso/macroporous SBA-15 monoliths and mesoporous SBA-15 powders were determined by nitrogen sorption using the BJH method based on the adsorption branch of the isotherm. The samples were degassed under vacuum at 180 °C for a minimum of 6 h prior to measurement of N_2 sorption isotherms at 77 K using a Micromeritics ASAP 2000 pore analyzer. Mean mesopore diameters for the various samples were estimated from the nitrogen sorption data using BET analysis (4V/A) and were verified by transmission electron microscopy (TEM) using a JEOL 2000FX microscope. The macropore structure was characterized by scanning electron microscopy (SEM), performed on a JEOL 6300 scanning electron microscope. Bulk Si/Al molar ratios were determined by inductively coupled plasma (ICP) elemental analyses.

Single-pulse solid-state ^{27}Al nuclear magnetic resonance (NMR) spectra were acquired using a Bruker AVANCE-300 NMR spectrometer operating at -18.1957 MHz, under conditions of magic-angle spinning (MAS). A 90° pulse length of 7.5 µs and 2-s recycle delays were used, with a 14-kHz sample spinning rate. ^{27}Al chemical shifts are referenced to an aqueous solution of $Al(NO_3)_3$. Quantitative comparisons of ^{27}Al signal intensities were made by measuring equivalent amounts of as-synthesized and calcined samples using a solid piece of aluminum nitride (AlN) as an internal standard, as described in Ref. [24]. Pulsed-field gradient ^{1}H NMR (PFG NMR) experiments were performed on a Bruker AVANCE-500 NMR spectrometer operating at 500.1324 MHz. Experiments were conducted at 25 °C using a stimulated-echo bipolar gradient pulse sequence [25,26], with 2-ms gradient pulses separated by 100-ms intervals. The applied gradient strength was varied from 2 to 95% of the 70 G/cm available.

2.3. Alkylation of aromatic compounds

All alkylation reactions were carried out in a continuously stirred batch reactor under reflux conditions using a three-neck 100-mL round-bottom flask equipped with a condenser, a nitrogen inlet for retaining an inert atmosphere, an outlet for product withdrawal, and a thermometer port for monitoring the temperature during reaction. The reactions were initiated by adding the various catalysts to boiling mixtures of benzyl alcohol (BzOH), which acted as an alkylating agent, and the respective aromatic compound for alkylation. All reactions (except that involving styrene, due to a potentially competing polymerization reaction) were conducted with an excess of the alkylating aromatic compound at its respective normal boiling point. The alkylation reaction temperatures for toluene, ethylbenzene, and cumene were thus 110, 136, and 152 °C, respectively. For a typical reaction, 20 mL of a given aromatic species (~ 0.2 mol) was mixed with approximately 8.0×10^{-3} mol BzOH; the amount of catalyst used was adjusted to maintain an approximately equivalent Al/BzOH mole ratio of 0.010 for all reactions. To prevent the rapid polymerization of styrene monomers expected in pure styrene near its boiling point (145 °C), styrene alkylation was carried out in a solution of low-boiling cyclohexane (boiling point 81 °C) with a molar ratio of 1 styrene:5 cyclohexane. The following reagents were used as received: benzyl alcohol (99+%, Aldrich),

toluene (ACS grade, EM Science), ethylbenzene (99.8%, anhydrous, Aldrich), cumene (99.9%, Fisher Acros), and cyclohexane (99+%, Fisher Acros). Styrene (99%, Aldrich) was distilled to remove inhibitor before use. To monitor the conversion, products were removed in small quantities from the reactor at specified time intervals and analyzed using gas chromatography on an HP5880A chromatograph.

Starting with fresh catalyst, each reaction was allowed to proceed to approximately complete conversion of the benzyl alcohol, after which the respective catalysts were reclaimed for reuse. All reused catalysts were dried in air (after filtration in the case of powders) before being added to a fresh reactant mixture that was identical in composition to the first.

3. Results and discussion

3.1. Catalyst properties

A photograph of a calcined meso/macroporous aluminosilica SBA-15 monolith (Si/Al = 72) prepared by emulsion- and block-copolymer templating is shown in Fig. 1a. The shape and size of the monoliths resemble those of the containers in which they are prepared and can be several centimeters in size or larger, as shown in the figure. The SEM image in Fig. 1b is representative of these monoliths; the macropores are tightly packed and are highly interconnected, with windows opening from each macropore into its surrounding neighbors. The macropores are reasonably monodisperse; for the particular sample shown, they are approximately 0.30 ± 0.05 µm. These centimeter-sized meso/macroporous SBA-15 monoliths were prepared with approximately 0.05-µm-thick macropore walls comprised of hexagonally ordered mesopores. Indeed, further magnification of the aluminosilica macropore framework using TEM (Fig. 1c) confirms the hexagonal arrangement of mesopores, as organized by the self-assembling P123 triblock copolymer species. From this and similar micrographs, the mesopores are observed to be about 5.7 nm in diameter, consistent with the value of 5.5 nm measured from the BET sorption isotherm. Such mesostructural ordering was similar to the uniform 5.2-nm-diameter hexagonally ordered mesopores in the aluminosilica SBA-15 powder. The small-angle X-ray diffraction spectrum (not shown) collected for the aluminosilica SBA-15 powder was typical of hexagonally ordered mesoporous materials, as observed previously [22,27] for siliceous samples, with one sharp peak corresponding to a d_{100} spacing of 9.0 nm and two smaller peaks indexed to d_{110} and d_{200} spacings of 5.1 and 4.5 nm, respectively. A single broad peak with a d_{100} spacing of 10.2 nm, similar to that of aluminosilica SBA-15, was observed for the meso/macroporous monolith. The absence of higher order peaks indicates that long-range ordering was reduced in the meso/macroporous materials, possibly due to influences of the macrostructure or emulsion synthesis conditions.
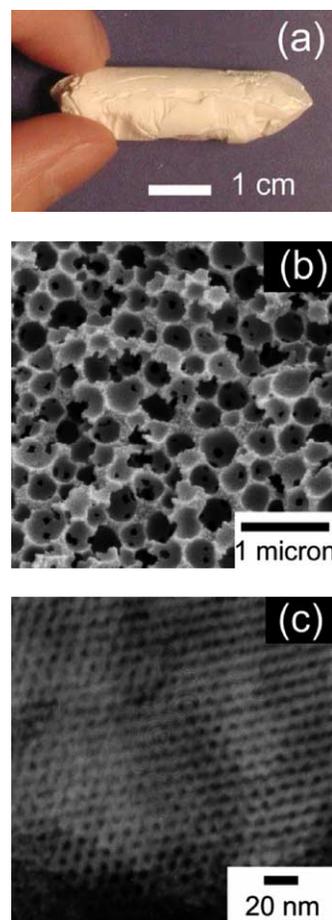

Fig. 1. (a) Optical photograph of a calcined aluminosilica meso/macroporous SBA-15 monolith and corresponding (b) SEM and (c) TEM micrographs showing the emulsion-templated macropores and block-copolymer-templated mesoporous wall structures, respectively.

Table 1
Physical and compositional properties of various aluminosilica catalysts

Catalysts	Surface area (m²/g)	Pore diameter (nm)	Bulk Si/Al ratio
Meso/macroporous SBA-15	860 ± 30	5.5 ± 0.4 300 ± 50	72 ± 6
Mesoporous SBA-15	870 ± 30	5.2 ± 0.4	70 ± 5
Zeolite Beta[a]	650	0.56	75

[a] Values are from vendor product specifications. Pore diameter is based on the smallest channel dimension.

For the purpose of examining the effects of pore size and structure on alkylation activity, aluminosilica meso/macroporous and mesoporous SBA-15 catalysts were synthesized with Si/Al ratios and surface areas that were similar to those for the crystalline nanoporous zeolite Beta sample used. Typical values for surface areas, mean mesopore diameters, and bulk Si/Al ratios for the meso/macroporous aluminosilica SBA-15 monoliths, as well as for the mesoporous SBA-15 and zeolite Beta powders, are summarized in Table 1. Bulk Si/Al ratios for the meso/macroporous SBA-15 monoliths, mesoporous SBA-15, and zeolite Beta were

72, 70, and 75, respectively, with corresponding surface areas of 856, 867, and 650 m^2/g. The calcined mesoporous SBA-15 powders had a broad distribution of particle sizes (SEM micrograph not shown) ranging from 1 to 100 µm. By comparison, crystalline zeolite Beta had much smaller highly uniform nanopores, 0.56 nm in the smallest channel dimension, and was in the form of a fine powder with particles ranging from 1 to 20 µm. The average particle sizes were estimated to be 25 and 10 µm for SBA-15 and zeolite Beta powders, respectively. For the pellet catalysts, SEM micrographs (not shown) of the surface and interiors of the SBA-15 and zeolite Beta pellets showed uniform densities with no evidence of large voids (micrometer size). The significant differences in the macroscopic morphologies and pore sizes of the five catalysts are important for understanding their Friedel–Crafts alkylation activities as discussed below.

Solid-state ^{27}Al MAS NMR was used to assess the types and relative fractions of different aluminum sites in the meso/macroporous and mesoporous SBA-15 materials. Of particular interest are tetrahedrally coordinated aluminum species associated with acidic framework sites that are active for alkylation [3]. ^{27}Al MAS NMR spectra (see Supplemental Information) acquired for the calcined aluminosilica meso/macroporous SBA-15 monolith, mesoporous SBA-15 powder, and nanoporous zeolite Beta powder show well-resolved peaks at chemical shifts of ~ 0 and ~ 50 ppm, which are attributed to octahedrally (Al^{VI}) and tetrahedrally (Al^{IV}) coordinated ^{27}Al species, respectively [28]. Integration of the ^{27}Al MAS peaks reveals that the percentages of tetrahedrally coordinated aluminum species relative to the total visible ^{27}Al species present ($Al^{IV} + Al^{VI}$) for the calcined meso/macroporous SBA-15 monolith, mesoporous SBA-15 powder, and zeolite Beta were 93, 91, and 98%, respectively.

Bulk elemental analyses, together with quantitative comparisons of ^{27}Al MAS signal intensities measured for the as-synthesized and calcined materials, however, indicate that the ^{27}Al signals measured may not account for all of the aluminum species present in the materials. Indeed, a recent study of related aluminosilica M41S materials showed that the amount of tetrahedrally coordinated aluminum characterized by ^{27}Al MAS NMR of calcined products was significantly reduced from that measured in as-synthesized samples, presumably due to conversion of aluminum species into so-called "NMR invisible" ^{27}Al upon calcination [24]. Quantitative ^{27}Al NMR "spin counting" in the meso/macroporous SBA-15 monoliths and powders establishes that, while the bulk Al concentrations of the samples remain unchanged, the total ^{27}Al NMR signal intensities decreased significantly, following calcination of the as-synthesized samples. These results are tabulated in Table 2. The differences in percentage ^{27}Al signal reduction among the meso/macroporous SBA-15 monoliths (55%), mesoporous SBA-15 powders (24%) and MCM-41 powders (50%) are thought to be due to their different synthesis con-

Table 2
Percentage of tetrahedrally coordinated Al characterized by ^{27}Al MAS NMR for aluminosilica SBA-15 catalysts

Catalysts	% Al^{IV} vs total ($Al^{IV} + Al^{VI}$)		Total ^{27}Al signal reduction[c]
	As synthesized[a]	Calcined[b]	
Meso/macroporous SBA-15	88%	93%	55%
Mesoporous SBA-15	80%	91%	24%

[a] ^{27}Al MAS NMR spectra not shown.
[b] See Supplemental Information.
[c] Quantitative decrease in total ^{27}Al MAS signal intensity associated with tetrahedrally and octahedrally coordinated aluminum species upon calcination.

ditions. For example, the use of alcohol (for the removal of the macropore-directing emulsion oil droplets) is expected to alter the local chemical environment near the Al species, due to its dehydrating effect. For the as-synthesized meso/macroporous SBA-15 monoliths and powder, the percentages of tetrahedrally coordinated aluminum with respect to the visible ^{27}Al NMR signals are estimated to be 88 and 80%, respectively. The results of the ^{27}Al NMR experiments, in conjunction with the bulk Al contents, allow the number of acid sites per mass of catalyst to be estimated. More specifically, the relative alkylation activities of different catalysts can be compared, based on the ratio of the number of active sites per mass of catalyst used to the amount of the limiting reactant in the batch feed, in this case, benzyl alcohol (BzOH). This acid site (Al^{IV})/BzOH ratio was kept constant at 0.010 ± 0.001. The concentrations of acid sites, and thus the Al/BzOH ratios, were estimated from the percentage of tetrahedrally coordinated Al species of the as-synthesized samples obtained by ^{27}Al MAS NMR.

3.2. Alkylation of aromatics

Friedel–Crafts alkylation of aromatic compounds can be represented schematically in Scheme 1 [reaction (1)] [1,29], where R is an aliphatic substituent, such as methyl, ethyl, isopropyl, or vinyl (ethenyl) group corresponding to toluene, ethylbenzene, cumene, or styrene, respectively. (The bond protruding to the center of the benzene ring in the product indicates that various isomers can be formed.) Alkylation of the single-ring aromatic compounds with benzyl alcohol proceeded with high to moderate conversion rates over the meso/macroporous aluminosilica SBA-15 monolith catalysts. Fig. 2 shows conversion plots for batch alkylation reactions of toluene, ethylbenzene, cumene, and styrene with benzyl alcohol. As can be seen from the figure, benzyl alcohol was consumed essentially to completion for each of the batch processes in less than 100 min, under conditions where the aromatic reactants were present in excess and kept at their respective boiling points (except for styrene). Alkylation of cumene, which took place at the highest temperature (152 °C), proceeded fastest, with the conversion of the limiting benzyl alcohol species being completed in less
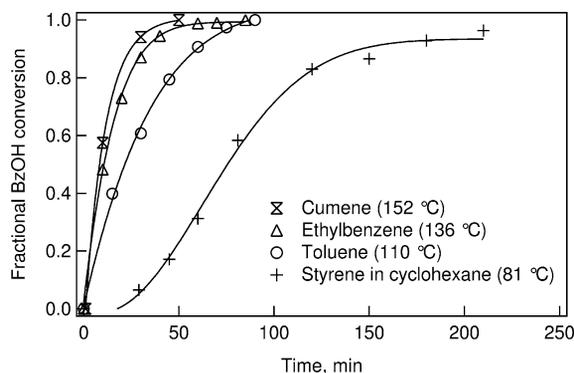
Fig. 2. Conversion of benzyl alcohol (BzOH) plotted as a function of time in a batch reactor for alkylation of various single-ring aromatic compounds using identical aluminosilica meso/macroporous SBA-15 monoliths (Si/Al = 72), Al/BzOH = 0.010.

than 50 min. This was followed by the rate of benzyl alcohol conversion in the presence of ethylbenzene at 136 °C, which was completed in ∼ 60 min, and toluene at 110 °C, which required ∼ 100 min. The reaction of benzyl alcohol with styrene was carried out in cyclohexane at the boiling point of the solvent (81 °C) to prevent unwanted competitive formation of polystyrene. Under these conditions, the styrene reaction required approximately 4 h to convert all of the benzyl alcohol. The relative reaction rates (R_i), which followed the sequence: $R_{cumene} > R_{ethylbenzene} > R_{toluene} > R_{styrene}$, correlated with the reaction temperatures at the boiling points of respective mixtures, and is consistent with the high endothermicity of Friedel–Crafts alkylations [29].

3.3. Comparison of catalysts

The activity of the meso/macroporous aluminosilica SBA-15 monolith for the alkylation of toluene with benzyl alcohol was compared to that of nanoporous crystalline zeolite Beta and mesoporous aluminosilica SBA-15 under the same reaction conditions (at 110 °C) to examine the differences in the intrinsic reaction rates and the role of diffusive resistances to mass transfer. The alkylation of toluene is chosen for comparison for practical reasons, such as its moderate boiling point (110 °C) and the accuracy of conversion rate measurements under the reaction conditions used. Zeolite Beta has been reported to catalyze liquid-phase alkylation reactions and showed good catalytic activity, compared to other zeolites, in the alkylation of benzene [5,30]. It thus, represents a good benchmark alkylation catalyst for comparison with the meso- and meso/macroporous solids. Mesoporous aluminosilica SBA-15, which has similar mesostructural characteristics (surface area, pore size, mesopore ordering) to that of the meso/macroporous aluminosilica monolith, was chosen for comparison to evaluate the influence of the bimodal meso/macropore structure. The three catalyst types differ not only in their apparent activities and pore structures, but also in their mean bulk dimensions. The bulk size differences are significant, ranging from mi-

crometers for the zeolite Beta and mesoporous powders to centimeters for the meso/macroporous monoliths. These differences lead to significant disparities in the rates at which reactants and products diffuse to and from the active sites within the catalysts.

To examine the differences in intrinsic reaction rates and the relative roles of mass transfer limitations within the bulk catalysts, zeolite Beta and mesoporous SBA-15 powders were formed into pellets with dimensions comparable to the meso/macroporous monoliths. The pressure used to press the pellets (120 MPa) was sufficiently high that the micrometer-size interparticle voids were dramatically reduced to ca. < 50 nm, based on SEM and BET results. The overall transport resistance experienced by molecules within the pellets is determined principally by diffusion within the mesopores. Thus, five catalysts were included in the comparison: a meso/macroporous aluminosilica SBA-15 monolith, mesoporous aluminosilica SBA-15 powder and pellet, and nanoporous zeolite Beta powder and pellet.

The conversions of benzyl alcohol in the batch alkylation of toluene for the five different catalysts are plotted as functions of time in Fig. 3. As discussed above, nearly complete conversion of benzyl alcohol (> 99%) was achieved in ∼ 100 min for the aluminosilica meso/macroporous SBA-15 monolith. By comparison, conversion of benzyl alcohol over mesoporous aluminosilica SBA-15 powder, under identical conditions, occurred more rapidly, being essentially complete after 15 min. However, when the same reaction was performed using the same mesoporous aluminosilica SBA-15 powder, but pressed into the form of a pellet, the rate of benzyl alcohol conversion was reduced significantly to a value below that of the meso/macroporous monolith (∼ 100% conversion after 120 min). A similar and even more pronounced effect of diffusion limitations was observed for alkylation of toluene over zeolite Beta in the form of a powder versus a pressed pellet in a well-stirred batch reactor. When micrometer-size crystallites of zeolite Beta powder were used, a conversion of greater than 90% of the benzyl alcohol was achieved in 45 min, compared to a con-
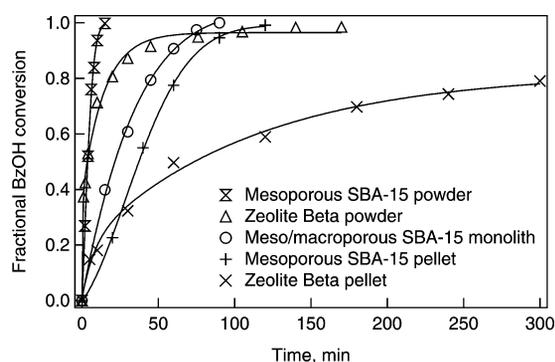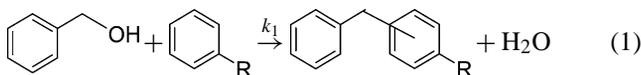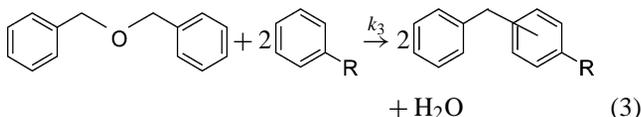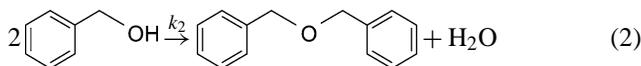

Fig. 3. Conversion of benzyl alcohol plotted as a function of time for the alkylation of toluene using various freshly calcined and activated aluminosilica catalysts in the forms of powders, pellets, and monoliths, Al/BzOH = 0.010, $T = 110$ °C.

Scheme 1.

Scheme 2.

version of 80% reached in 300 min for the same zeolite Beta powder pressed into a dense pellet. To characterize and better understand the differences in the conversion times observed for the five catalysts, a simple quantitative model is developed and discussed below.

3.4. Alkylation reaction model

Two reaction schemes have been proposed for the alkylation of toluene with benzyl alcohol [31]: Scheme 1 [reaction (1)] involves the direct formation of benzyl toluene (BT) by alkylation of toluene with benzyl alcohol; Scheme 2 [reactions (2) and (3)] involves a two-step process where benzyl ether (BE) is formed first and subsequently converted to BT. GC analyses of the product mixtures indeed confirmed the existence of benzyl ether at intermediate batch reaction times (see Section 3.6), which suggests that Scheme 2 plays a role in the process.

In reactions (1), (2), and (3), k_1, k_2, and k_3 are the corresponding apparent net forward reaction rate coefficients. Higher order alkylation reactions (which yield polyalkylated products) are not taken into account. However, the simple quantitative model developed below, taken together with experimental data, suggests that these higher order reactions do not play a central role and that the reactions above capture the essential features of the overall kinetics.

The rate equations that correspond to the set of reactions in Schemes 1 and 2 are given by

$$\frac{dC_{BzOH}(t)}{dt} = -k_1 C_{BzOH}(t) - k_2 C_{BzOH}^2(t), \tag{4}$$

$$\frac{dC_{BT}(t)}{dt} = k_1 C_{BzOH}(t) + 2k_3 C_{BE}(t), \tag{5}$$

$$\frac{dC_{BE}(t)}{dt} = \frac{k_2}{2} C_{BzOH}^2(t) - k_3 C_{BE}(t), \tag{6}$$

where $C_{BzOH}(t)$, $C_{BT}(t)$, and $C_{BE}(t)$ are the concentrations (mol/L) of benzyl alcohol, benzyl toluene, and benzyl ether, respectively, at time t. These equations are solved numerically using the initial conditions $C_{BzOH}(0) = C_{BzOH}^0$ and $C_{BT}(0) = C_{BE}(0) = 0$. For the case of benzyl alcohol, an

analytical solution can be obtained,

$$\frac{C_{BzOH}}{C_{BzOH}^0} = \frac{\kappa_1}{(\kappa_1 + \kappa_2)e^{\kappa_1 t} - \kappa_2}$$

$$\approx 1 - (\kappa_1 + \kappa_2)t + O(t^2) \quad \text{for small } t, \tag{7}$$

where $\kappa_1 = k_1$, $\kappa_2 = k_2 C_{BzOH}(0)$, and $\kappa_3 = k_3$ are characteristic reaction rate coefficients in s^{-1} and the quantity $(\kappa_1 + \kappa_2)$ is the initial rate of disappearance of benzyl alcohol.

The *normalized* time-dependent concentration profiles (in mole fractions) of BzOH, BT, and BE measured for the toluene alkylation reactions over the meso/macroporous aluminosilica SBA-15 monolith, mesoporous aluminosilica SBA-15 powder, and zeolite Beta powder catalysts are shown in Fig. 4, together with fits to the model. As shown in Fig. 4, for each of the three catalysts examined, the concentration of benzyl alcohol decreased rapidly initially, followed by a slower decay until nearly all of the benzyl alcohol was consumed. The concentration of benzyl toluene increased with time and reached the highest value at the end of the reaction. In contrast, the concentration of benzyl ether reached a maximum before complete conversion of benzyl alcohol and decreased during the remainder of the reaction time. All of these distinct features are captured by the model based on reactions (1)–(3). The transient concentrations predicted by the model also agree quantitatively well with the experimental data for all of the catalysts examined.

The rate coefficients, obtained by fitting the model to the experimental data, for all five catalysts are presented in Table 3. The fastest rate of direct alkylation (largest κ_1) is obtained for mesoporous aluminosilica SBA-15 powder ($1.5 \times 10^{-3} \ s^{-1}$), which is five times greater than that for the same SBA-15 powder pressed into the form of a pellet ($3.0 \times 10^{-4} \ s^{-1}$). Similarly, for zeolite Beta, the value of κ_1 obtained for the powdered catalyst ($8.0 \times 10^{-4} \ s^{-1}$) is more than 10 times greater than that obtained in the form of a pellet ($6.5 \times 10^{-5} \ s^{-1}$). The meso/macroporous SBA-15 monolith yielded a value for κ_1 of $5.0 \times 10^{-4} \ s^{-1}$, which is intermediate between the values observed for the mesoporous SBA-15 powder and pellet samples. Thus, the sequence of catalyst materials from the fastest to slowest apparent alkylation rates is mesoporous SBA-15 powder > zeolite Beta powder > meso/macroporous SBA-15 monolith > mesoporous SBA-15 pellet > zeolite Beta pellet.

The same sequence is observed for the rate coefficient for the production of benzyl ether, κ_2 and for the sum $\kappa_1 + \kappa_2$. Not surprisingly, the sequence of values for $\kappa_1 + \kappa_2$, which accounts for the initial disappearance of benzyl alcohol, follows the same order as the times required for reaching 80% BzOH conversion for the five different catalysts. The sequence of values for κ_3, which describes how fast the intermediate (benzyl ether) is converted to the desired product (benzyl toluene), follows a different order: mesoporous SBA-15 powder > meso/macroporous SBA-15 monolith > mesoporous SBA-15 pellet, zeolite Beta pellet > zeolite
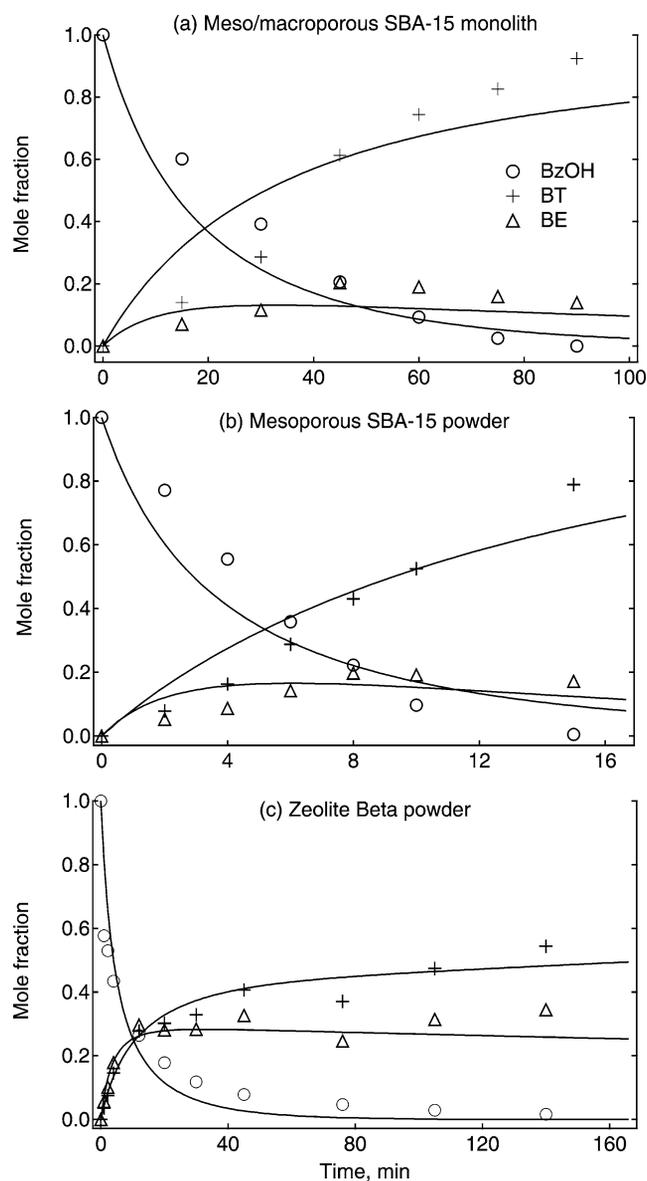
Fig. 4. Normalized concentrations (with respect to the initial BzOH concentration) of benzyl alcohol (BzOH), benzyl toluene (BT), and benzyl ether (BE) as functions of batch reaction time for toluene alkylation with BzOH over three aluminosilica catalysts: (a) meso/macroporous SBA-15 monolith, (b) mesoporous SBA-15 powder, and (c) zeolite Beta powder. Solid lines represent predictions from the model proposed. Al/BzOH = 0.010, $T = 110\,°C$.

Beta powder. The small values of κ_3, which are consistently smaller than either κ_1 or κ_2 for all catalysts, indicate that reaction (3) is relatively slow. The importance of the relative values of the various rate coefficients and their effects on product selectivity for the respective catalysts are discussed below.

3.5. Role of diffusion

The observation that the rates of conversion of benzyl alcohol for the powdered catalysts are significantly faster than for the pellets or monoliths suggests that diffusion limitations may play a role in determining the overall rates of conversion. The Thiele modulus ϕ provides a convenient nondimensional measure of the importance of diffusion on the apparent conversion rates. It is defined as the square root of the ratio of an intrinsic reaction rate to a diffusion rate (D/R^2) within the catalyst particle [32]. When diffusion is slow (i.e., $\phi \gg 1$), transport limitations make the measured overall reaction rates slow compared to the intrinsic reaction rates. For sufficiently small particles, however, diffusive mass transport into the particles is rapid enough ($\phi < 1$) that the measured reaction rate coefficients κ_1 and κ_2 are equal to their respective intrinsic reaction rate coefficients. Thus, to assess the role of diffusion in limiting the conversion of benzyl alcohol in the pellet and monolithic catalysts, the rate coefficients for the powder samples are taken to be equal to the intrinsic reaction rates for the purpose of determining the Thiele moduli.[1] Furthermore, because the initial rate at which benzyl alcohol disappears is given by $\kappa_1 + \kappa_2$ (see Section 3.4), this sum can be used to evaluate the Thiele moduli for the various catalysts. Therefore, for the analysis below,

$$\phi = R\sqrt{\frac{\kappa_{1,s} + \kappa_{2,s}}{D}}, \qquad (8)$$

Table 3
Rate coefficients κ_i, Thiele moduli ϕ, and effectiveness factors η for five aluminosilica catalysts for the batch alkylation of toluene with benzyl alcohol at 110 °C

Catalyst	κ_1 (s^{-1})	κ_2 (s^{-1})	κ_3 (s^{-1})	ϕ	η
Meso/macroporous SBA-15 monolith	5.0×10^{-4}	5.5×10^{-4}	1.0×10^{-4}	5.9	0.31
SBA-15 powder	1.5×10^{-3}	3.5×10^{-3}	9.0×10^{-4}	0.28	~ 1
SBA-15 pellet	3.0×10^{-4}	3.0×10^{-4}	8.0×10^{-5}	6.7	0.28
Zeolite Beta powder	8.0×10^{-4}	3.0×10^{-3}	1.5×10^{-5}	1.0	0.94
Zeolite Beta pellet	6.5×10^{-5}	8.0×10^{-5}	5.5×10^{-5}	> 100	< 0.01

where R is the radius in [m] of a nominally spherical bulk catalyst particle/pellet/monolith $\kappa_{1,s}$ and $\kappa_{2,s}$ are the normalized intrinsic reaction rate constants in [s^{-1}], and D is the diffusion coefficient of a reactant species within the bulk catalyst in [m^2 s^{-1}].

Using these reaction rate coefficients, the Thiele moduli can be computed for the five catalysts, provided the diffusion coefficients of benzyl alcohol within the catalyst particles are known. To determine these diffusion coefficients, standard pulsed-field gradient ^{1}H NMR measurements were employed. Diffusion coefficients of benzyl alcohol in perdeuterated toluene were measured to be 2.8×10^{-9} and 3.6×10^{-9} m^2 s^{-1} for the mesoporous SBA-15 pellet and meso/macroporous SBA-15 monolith, respectively.[2] It is interesting to note that the diffusion coefficient in the meso/macroporous SBA-15 sample is larger than that in the strictly mesoporous SBA-15 pellet. As the only difference in the samples is the sizes of their respective macropores, it is reasonable to attribute the faster diffusion in the meso/macroporous monolith to the presence of the more open macropores.

Similar direct experimental measurements of the intraparticle diffusivity of benzyl alcohol in mesoporous SBA-15 and nanoporous zeolite Beta powders were not possible, due to their significant fraction of particles with small dimensions (< 5 μm) and limited strengths of the magnetic field gradients. For PFG NMR to yield accurate intraparticle diffusion coefficients, the root-mean-square (r.m.s.) displacement of a diffusant during the time scale (~ 100 ms) of the PFG NMR measurement should be small compared to the size of the particles present, and this is not the case for substantial fractions of both the SBA-15 and the zeolite Beta powders. In addition, for the nanoporous molecular sieves, such as zeolite Beta, guest molecule diffusivities are typically much lower than in bulk fluids [33], so that PFG diffusion measurements are limited by the strengths of the applied magnetic field gradients (70 G/cm) to diffusivities $> 10^{-12}$ m^2 s^{-1}. The diffusivity of benzyl alcohol in zeolite Beta could not be measured and thus appears to be below this threshold at 25 °C. For these reasons, intraparticle diffusion coefficients for benzyl alcohol were estimated from literature values of similar species to be $\sim 10^{-13}$ m^2 s^{-1} for nanoporous zeolite Beta [34,35] and $\sim 10^{-11}$ m^2 s^{-1} for mesoporous SBA-15 [36] powders.

Using the reaction rates, catalyst dimensions, and diffusion coefficients obtained as described above, Thiele moduli for the five samples were computed and are tabulated in Table 3. SBA-15 powder catalysts have a small Thiele modulus $\phi \sim 0.28$, confirming that diffusion does not play a major role in limiting the overall reaction rate. By contrast, the reaction kinetics for all of the centimeter-size pellet/monolith catalysts fall well into the diffusion-limited regime ($\phi > 1$).

The Thiele modulus for the SBA-15 pellet ($\phi \sim 6.7$) is more than an order of magnitude larger than for the SBA-15 powder ($\phi \sim 0.28$). Thus, the large decrease in overall reaction rate when pellets are used in place of powders can be attributed to mass transfer limitations. For zeolite Beta, diffusion clearly limits the overall reaction rate in the pellet sample, as the Thiele modulus for the pellet ($\phi > 100$) is at least two orders of magnitude larger than for the powder ($\phi \sim 1.0$). In fact, diffusion cannot be entirely neglected even in the powder sample, for which the Thiele modulus is estimated to be approximately unity. This also means that the reaction rates measured for the zeolite Beta powder may be slightly lower than the true intrinsic reaction rate, and thus that the true Thiele moduli for the zeolite Beta samples may be somewhat higher than those reported here. This does not change the conclusions about the relative influences of diffusion on the rates of reaction measured for the powder and pellet samples.

The Thiele moduli for the aluminosilica meso/macroporous SBA-15 monolith ($\phi \sim 5.9$) and mesoporous SBA-15 pellet ($\phi \sim 6.7$) are similar. This is not surprising, as the macroscopic particle dimension and intrinsic reaction rates are similar and the diffusion coefficients of the reactant molecules are nearly the same for both catalysts. The modest enhancement of the alkylation rate for the meso/macroporous SBA-15 monolith catalyst compared to the SBA-15 pellet is consistent with slightly higher diffusivities in the larger macropores of the emulsion-templated meso/macroporous monolith.

While the Thiele modulus is useful in assessing the relative importance of diffusion, a more direct indication of the degree to which diffusion and macroscopic catalyst dimensions and shape influence the overall reaction rate is the effectiveness factor, which is defined as the ratio of the measured reaction rate to the reaction rate that would result if the entire surface were exposed to the surface concentration of reactants.[3] Values of η for the five catalyst samples studied are presented in Table 3 for toluene alkylation by benzyl alcohol at 110 °C. Mesoporous SBA-15 and zeolite Beta powders had effectiveness factors near unity, due to their small particle sizes. The effectiveness factor for the meso/macroporous monolith was found to be 0.31, similar to 0.28 for the mesoporous SBA-15 pellet. Diffusion resistances are expected to be negligible only for particles smaller than about 0.5 mm (for which η is estimated to be > 0.95), with the result that the effectiveness factors for the SBA-15 monoliths and pellets will be nearly the same. For the zeolite Beta pellet, η is small (< 0.01), as result of a fast intrinsic reaction rate and severe diffusive limitations to mass transfer.

---

[2] The diffusivities shown have been corrected for temperature using the Stokes–Einstein relation, including changes in viscosity, from values measured at 25 °C to the reaction temperature of 110 °C.

[3] The effectiveness factor η can be related to ϕ for certain known geometries [37]. The pellets and monolith are well approximated as cylinders or disks, while the particles in the powder samples are approximated as spheres based on SEM images (not shown). Nevertheless, the dependence on sample shape is weak in the cases considered here, where the diameters and lengths of the cylinders/disks are comparable.

Thus, diffusion appears to exert important influences on the measured alkylation rates of toluene for the three macroscopic pellet/monolith catalysts: the zeolite Beta and SBA-15 pellets and the meso/macroporous SBA-15 monolith. Among these systems, the available active sites in the meso/macroporous monolith are more effectively utilized for toluene alkylation than active sites in the SBA-15 or zeolite Beta pellets. The slightly larger effectiveness factor (and thus smaller ϕ) can be attributed in part to faster diffusion of reactant species within the meso/macroporous monolith, as a result of its open macroporous network. Finally, for the SBA-15 and zeolite Beta powders, diffusion limitations appear not to play a significant role in the rates at which toluene is catalytically alkylated, as indicated by their effectiveness factors of approximately unity.

3.6. Catalyst selectivities

In addition to differences in batch alkylation reaction rates, the selectivities of the aluminosilica meso/macroporous SBA-15 monolith, mesoporous SBA-15 powder, and zeolite Beta powder for the formation of benzyl toluene were examined. Analyses of the product mixtures by gas chromatography revealed the formation of several product species during the batch reactions, consistent with reactions (1)–(3). Two principal isomers (*para* and *ortho*) of benzyl toluene (BT) were observed for all reactions of toluene with benzyl alcohol, consistent with the *para/ortho*-directing tendencies of alkyl groups [29]. In addition to the desired benzyl toluene species, benzyl ether was also detected in significant fractions as a major side product for each of the catalysts. As illustrated by reactions (2) and (3) above, benzyl ether can be formed by reaction of two benzyl alcohol molecules. Selectivity for the desired alkylated product (both BT isomers) was determined as a fraction of the combined BT and BE species, near complete conversion of BzOH. No preferential formation of the *para* or *ortho* isomers of benzyl toluene (near complete conversion of BzOH) was observed for the SBA-15 catalysts. This is not surprising for small-molecule species reacting in the relatively large mesoporous channels. These results appear to be independent of catalyst preparation.

For the aluminosilica meso/macroporous SBA-15 monoliths, the concentration of benzyl alcohol decreases monotonically with reaction time, as can be seen in Fig. 4a. The alkylated product, benzyl toluene, increases steadily throughout reaction, while benzyl ether slowly increases to a maximum (0.21 mole fraction) and then decreases with reaction time as it converts to the desired benzyl toluene product. The concentration of benzyl ether remains consistently lower than that of benzyl toluene throughout the course of the reaction. The selectivity for BT is found to be 93%, as the conversion of BzOH approaches completion. Mesoporous aluminosilica SBA-15 powders exhibit the same concentration trends as the meso/macroporous SBA-15 monoliths, as shown in

Fig. 4b, though with lower selectivity for BT, 79%, near complete conversion of the benzyl alcohol.

In contrast, when the concentrations of BzOH, BT, and BE are plotted versus batch alkylation time in the presence of zeolite Beta powder (Fig. 4c), significantly different results are obtained. Most noticeable is the relatively high concentration of BE side product produced (0.30 mole fraction), which contributes ultimately to a lower selectivity (59%) for the desired benzyl toluene product. The BE concentration is higher than that of BT during the first 15 min of reaction during which most of the BzOH is consumed. Its concentration also remains relatively constant throughout the remainder of the reaction. This suggests that BE does not undergo further reaction to a significant extent in the presence of zeolite Beta to produce BT, as observed for aluminosilica meso/macroporous SBA-15 monolith and mesoporous SBA-15 powder.

Mesoporous aluminosilica SBA-15 powders and meso/macroporous aluminosilica SBA-15 monoliths have similar mesopore sizes and surface acid sites and exhibit similar reaction properties with respect to BzOH, BT, and BE. In contrast, crystalline zeolite Beta has stronger acid sites and smaller pores, both of which may influence selectivity. The low selectivity toward BT observed for zeolite Beta can be explained by the various reaction rate coefficients. Referring to the values listed in Table 3, one important feature is different among the various catalysts. In the case of zeolite Beta powder, the rate coefficient for the formation of benzyl ether, κ_2, is significantly higher than both rate coefficients κ_1 and κ_3 associated with the formation of benzyl toluene. By comparison, the values of κ_1, κ_2, and κ_3 for the mesoporous and meso/macroporous SBA-15 catalysts are similar in magnitude. This indicates that reaction (2) is important for zeolite Beta and that the overall reaction proceeds predominantly by Scheme 2 to form benzyl ether, instead of by direct alkylation (Scheme 1) to form BT. Furthermore, the subsequent reaction rate coefficient, κ_3 is small (1.5×10^{-5} s^{-1}), indicating that conversion of BE to BT occurs significantly more slowly. Consequently, the yield of benzyl toluene over the zeolite Beta powder catalyst is relatively low. This explanation is supported by the relatively high mole fraction (~ 0.3) of BE observed, which once reached, remained high throughout the reaction, as shown in Fig. 4c. For the case of the meso/macroporous SBA-15 monolith and mesoporous SBA-15 powder, κ_3 is comparable in magnitude to the values for κ_1 and κ_2, with all three reactions appearing to contribute significantly to the formation of benzyl toluene.

The strong acidity or small pore sizes of zeolite Beta may contribute to the absence of significant conversion of benzyl ether to benzyl toluene. The molecular dimensions of the nanopores may interfere with the formation of key transition state species, as thought to occur for the reactions of *ortho*- and *meta*-xylene in the zeolite ZSM-5 [38]. During the initial formation of BE and BT, other undesirable products (e.g., coke) may also form and become immobilized and block access to the strong acid sites. The issue of

catalyst deactivation is examined in more detail below. The aluminosilica meso/macroporous SBA-15 monoliths exhibit significantly higher batch selectivity for the desired benzyl toluene product (93%) than the mesoporous SBA-15 (79%) or the nanoporous zeolite Beta (59%) powders, even though the latter achieves more rapid conversion.

3.7. Catalyst deactivation

Deactivation properties of the aluminosilica meso/macroporous SBA-15 monolith, mesoporous SBA-15 powder and pellet, and zeolite Beta powder catalysts were examined for a series of consecutive toluene/benzyl alcohol batch alkylation reactions performed without replacing or reactivating the catalysts. The relative activities of the meso/macroporous SBA-15 monolith and zeolite Beta powder, expressed as the fractional conversion of benzyl alcohol, are shown in Fig. 5 as functions of batch reaction time. Data for the SBA-15 powder and pellet samples are not included to avoid clutter; the data from these samples fall in between the data for the meso/macroporous monolith and zeolite Beta powder. The salient features of the deactivation behaviors of the different catalysts, including the SBA-15 powder and pellet samples, are summarized in Table 4, where the reaction times to reach 80% BzOH conversion for each subsequent batch are tabulated. In addition, the fractions of activity compared to the fresh catalysts, defined to be the ratio of $(\kappa_1 + \kappa_2)$ of the reused catalysts to that of the fresh catalysts, are shown for each batch. The quantity $(\kappa_1 + \kappa_2)$ is used as the basis for calculating the activity, because it accounts for the overall rate at which most of the BzOH is converted.

Diverse deactivation behaviors were observed for the various catalysts studied. As shown in Table 4, the aluminosilica SBA-15 meso/macroporous monolith exhibited the slowest deactivation, as indicated by the fraction of original activity retained by the reused monolithic catalyst for five successive batches. The once-reused meso/macroporous monolith remained almost as active as the fresh catalyst, retaining 92% of its original activity. Further decreases were observed in the activities of reused meso/macroporous catalysts between subsequent consecutive batch reactions corresponding successively to 75, 63, and 55% of the activity of the fresh monolith. For the fifth reuse of the meso/macroporous monolith, 4 h were required to convert essentially all of the BzOH, or approximately twice the time required for the fresh catalyst.

By comparison, the mesoporous SBA-15 aluminosilica powder deactivated more rapidly than the meso/macroporous SBA-15 monolith, relative to the corresponding starting materials. The SBA-15 powder afforded higher conversion rates, achieving 80% conversion of benzyl alcohol in 5 and 6 min for the fresh and once-reused catalysts, respectively. However, a 25% decrease in the conversion rate was observed for the once-reused mesoporous SBA-15 powder compared to the fresh catalyst, in contrast to an 8% decrease for the meso/macroporous monolith. Similarly,
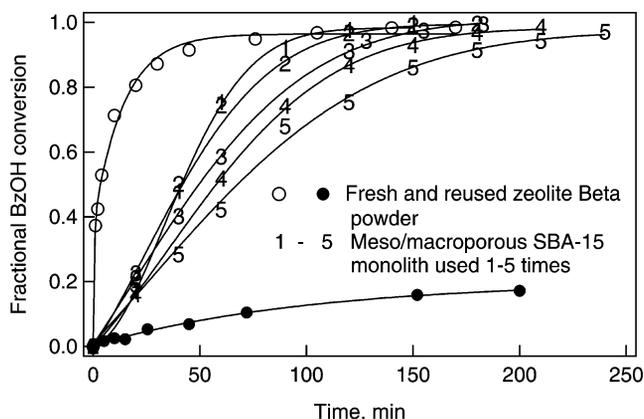

Fig. 5. Conversion of benzyl alcohol plotted as a function of time in a batch reactor for alkylation of toluene over freshly activated and reused aluminosilicate zeolite Beta powder (denoted by open and solid circles, respectively) and aluminosilica meso/macroporous SBA-15 monolith (denoted by 1–5 corresponding to the respective of number times used). All reused catalysts were recovered by filtration of the spent catalyst from the previous batch reaction. Al/BzOH = 0.010, $T = 110\,^{\circ}$C.

Table 4
Deactivation of various catalysts for successive batch alkylation of toluene with benzyl alcohol at $110\,^{\circ}$C

Catalyst	Time for 80% conversion of BzOH (min)	Fraction of fresh catalyst activity
Meso/macroporous monolith		
1	66	1.00
2	74	0.92
3	91	0.75
4	102	0.63
5	128	0.55
SBA-15 powder		
1	5	1.00
2	6	0.75
SBA-15 pellet		
1	92	1.00
2	128	0.76
Zeolite Beta powder		
1	18	1.00
2	> 200	0.006

for the case of the SBA-15 pellet, deactivation occurred more rapidly than for the meso/macroporous monolith, as well: 76% of the original activity was retained in the once-reused SBA-15 pellet, compared to 92% for the once-reused meso/macroporous monolith. Furthermore, the time required to convert 80% of the benzyl alcohol over the fresh SBA-15 pellet matched that of the meso/macroporous monolith used three times, and that for the once-reused SBA-15 pellet was equivalent to that of the meso/macroporous monolith used five times. The aluminosilica meso/macroporous SBA-15 monolith thus retained activity for Friedel–Crafts alkylation of toluene substantially longer than mesoporous SBA-15 pellet (discussed below).

For the case of zeolite Beta, Friedel–Crafts alkylation activity diminished much more rapidly and significantly than

for either the meso/macroporous SBA-15 monolith or the mesoporous SBA-15 powder and pellet. Most of the original activity of the zeolite Beta starting material was lost after only a single use, yielding a subsequent activity of 0.6% of the fresh zeolite Beta catalyst. Referring to Fig. 5, the fresh zeolite Beta powder was highly active, converting 80% of the benzyl alcohol to products in 18 min. However, a substantially reduced conversion of only $\sim 20\%$ was obtained in 200 min for a subsequent batch reaction that reused the zeolite Beta catalyst from the previous reaction. The rate of conversion of benzyl alcohol using the once-reused zeolite Beta catalyst was much lower (by more than an order of magnitude, based on the quantity $(\kappa_1 + \kappa_2)$) than that obtained for the meso/macroporous SBA-15 monolith catalyst after five uses.

To understand the differences in the rates of deactivation among the various catalysts, the origin (principally coking) of deactivation was examined. Coking occurs as a result of the formation and deposition of carbonaceous residues on the active catalyst surface, which leads to deactivation by pore-mouth blockage or by local poisoning of active sites. This is evidenced by the black appearance of the catalysts after reaction and calcination in an inert (oxygen-deficient) atmosphere. Under normal process conditions, such carbonaceous species tend to be irreversibly adsorbed, the severity of which depends on acid-site strength, pore dimensions, and particle size [39,40]. The deposited coke can be removed and catalysts regenerated by calcination in air at 500 °C for 4 h. BET measurements after reaction and regeneration confirmed virtually 100% recoveries of the original surface areas, porosities, and alkylation activities of all five catalysts examined in the present study.

Based on BET surface area analyses of the *deactivated* catalysts, pore blockages appeared to be present to a significant extent in all of the systems. Approximately 35% reductions in surface area were measured for the once-used meso/macroporous SBA-15 monolith and mesoporous SBA-15 pellet catalysts, indicating that the degrees of pore blockage were substantial. The slower deactivation in the meso/macroporous SBA-15 monolith, compared to the otherwise similar SBA-15 pellet, is attributed to the former's more open interconnected macroporous structure. The more open macropore network may provide alternate diffusion routes that facilitate mass transfer of reactant and product species in coked catalysts, thus enabling the monoliths to sustain higher activities for similar extents of coking. For the case of mesoporous SBA-15 powder, the rates of conversion of benzyl alcohol and deactivation are consistently higher than those found for the meso/macroporous SBA-15 monolith. Differences in the strengths of acid sites or sizes of the mesopore channels are unlikely to play significant roles in the reduced deactivation of the meso/macroporous SBA-15 monolith compared to the mesoporous SBA-15 powder and pellets, which were synthesized under similar conditions to yield essentially identical mesopore compositions and structures.

By comparison, zeolite Beta exhibited dramatically different deactivation behavior, consistent with coking at the strong acid sites, which is expected to be exacerbated by the small nanopores (0.56 nm), which are more prone to blockage [39]. Indeed, a reduction of approximately 50% was measured in the BET surface area of once-reacted zeolite Beta powder, compared to a drop of 35% in the BET surface areas of the SBA-15 samples, consistent with more severe pore blockage in zeolite Beta. However, pore blockage alone may not account for the acute deactivation behavior observed for the zeolite Beta catalysts. In fact, the strong acid sites in zeolite Beta samples are expected to intensify deactivation by local site poisoning, as well [39,40]. Together these contribute to the diminished activity of zeolite Beta for toluene alkylation, resulting in low conversion ($\sim 20\%$) of benzyl alcohol for the once-reused powder catalyst.

Based on the performance of reused catalysts, the aluminosilica meso/macroporous SBA-15 monoliths exhibited superior resistances to deactivation, compared to mesoporous SBA-15 and nanoporous zeolite Beta. The once-reused meso/macroporous SBA-15 monolith, mesoporous SBA-15 powder and pellet, and zeolite Beta powder catalysts retained 92, 75, 76, and 0.6%, respectively, of the original activities of the corresponding fresh starting materials. Deactivation by pore blockage appeared to be significant for each of the different catalysts, while deactivation by site poisoning likely also plays a significant role in the more strongly acidic zeolite Beta catalysts. In addition, the meso/macroporous catalysts retained their original monolithic forms even after five successive reactions under severe mixing conditions, demonstrating appreciable mechanical robustness. Preservation of the macrostructure was also confirmed by SEM with no significant shrinkage observed after successive reaction and regeneration steps. All of catalysts could be regenerated by calcination treatments in air to recover virtually all of their original activities.

4. Conclusions

Self-supporting mechanically robust aluminosilica SBA-15 monoliths (> 1 cm) with independently adjustable pores sizes in the micrometer and nanometer ranges have been synthesized using combined emulsion- and block-copolymer templating. The catalytic activities of these meso/macroporous SBA-15 monoliths were examined for Friedel–Crafts alkylation of single-ring aromatic compounds (toluene, cumene, ethylbenzene, and styrene), with the alkylation of toluene compared in detail with the activities of mesoporous aluminosilica SBA-15 and crystalline nanoporous zeolite Beta with similar Si/Al ratios. Compared to meso/macroporous SBA-15, fresh zeolite Beta and mesoporous SBA-15 powders showed higher activities for the alkylation of toluene, but were less selective (59 and 79%, respectively) for the alkylated product, benzyl toluene, than the

meso/macroporous monolith (93%). Lower overall toluene alkylation rates were also observed for centimeter-size pellets of mesoporous SBA-15 and zeolite Beta powders, compared to the meso/macroporous SBA-15 monoliths. The meso/macroporous SBA-15 monolith, mesoporous SBA-15 powder and pellet, and zeolite Beta powder were found to have effectiveness factors 0.3–1.0, compared to $\eta \sim 0.01$ for pelletized zeolite Beta. Diffusive resistances to mass transfer influence the apparent reaction rates for all of the monolithic and pelletized catalysts. Finally, the meso/macroporous aluminosilica SBA-15 monolith catalyst experienced reduced deactivation for Friedel–Crafts alkylation, compared to mesoporous SBA-15 and zeolite Beta powders.

Heterogeneous acid catalysis may benefit from monolithic meso/macroporous catalysts with independently adjustable mesopore and macropore dimensions and macroscopic morphologies, due to the sensitivity of catalytic reaction rates and selectivities to diffusive resistances to mass transfer. Such considerations have been shown to be important for the low-molecular-weight reactants and products discussed here and will play an even greater role for large macro- and biomolecular species. Meso/macroporous solids present opportunities to hierarchically design and engineer heterogeneous catalysts with improved control and integration of materials composition, structure, and performance.

Acknowledgments

References

[1] G.A. Olah, Friedel–Crafts Chemistry, Wiley, New York, 1973.
[2] R.M. Roberts, A.A. Khalaf, Friedel–Crafts Alkylation Chemistry: A Century of Discovery, Dekker, New York, 1984.
[3] A. Corma, Chem. Rev. 95 (1995) 559.
[4] K. Tanabe, W.F. Hölderich, Appl. Catal. A 181 (1999) 399.
[5] G. Bellussi, G. Pazzuconi, C. Perego, G. Girotti, G. Terzoni, J. Catal. 157 (1995) 227.
[6] C. Perego, S. Amarilli, A. Carati, C. Flego, G. Pazzuconi, C. Rizzo, G. Bellussi, Micropor. Mesopor. Mater. 27 (1999) 345.
[7] A. Corma, V. Martínez-Soria, E. Schnoeveld, J. Catal. 192 (2000) 163.
[8] S.N. Jun, R. Ryoo, J. Catal. 195 (2000) 237.
[9] R. Carranza, Chem. Process 62 (1999) 47.
[10] C. Ercan, F.M. Dautzenberg, C.Y. Yeh, H.E. Barner, Ind. Eng. Chem. Res. 37 (1998) 1724.
[11] D.Y. Zhao, P.D. Yang, B.F. Chmelka, G.D. Stucky, Chem. Mater. 11 (1999) 1174.
[12] H. Maekawa, J. Esquena, S. Bishop, C. Solans, B.F. Chmelka, Adv. Mater. 15 (2003) 591.
[13] P.D. Yang, T. Deng, D.Y. Zhao, P.Y. Feng, D. Pine, B.F. Chmelka, G.M. Whitesides, G.D. Stucky, Science 282 (1998) 2244.
[14] S.A. Davis, S.L. Burkett, N.H. Mendelson, S. Mann, Nature 385 (1997) 420.
[15] Q. Luo, L. Li, B. Yang, D.Y. Zhao, Chem. Lett. (2000) 378.
[16] D.H. Reeder, A.M. Clausen, M.J. Annen, P.W. Carr, M.C. Flickinger, A.V. McCormick, J. Colloid Interface Sci. 184 (1996) 328.
[17] V. Pedroni, P.C. Schulz, M.E.G. de Ferreira, M.A. Morini, Colloid Polym. Sci. 278 (2000) 964.
[18] A. Imhof, D.J. Pine, Nature 389 (1997) 948.
[19] B.T. Holland, C.F. Blanford, A. Stein, Science 281 (1998) 538.
[20] T.G. Mason, J. Bibette, Langmuir 13 (1997) 4600.
[21] P. Holmqvist, P. Alexandridis, B. Lindman, J. Phys. Chem. B 102 (1998) 1149.
[22] P.Y. Feng, X.H. Bu, D.J. Pine, Langmuir 16 (2000) 5304.
[23] P.Y. Feng, X.H. Bu, G.D. Stucky, D.J. Pine, J. Am. Chem. Soc. 122 (2000) 994.
[24] M.T. Janicke, C.C. Landry, S.C. Christiansen, S. Birtalan, G.D. Stucky, B.F. Chmelka, Chem. Mater. 11 (1999) 1342.
[25] D.H. Wu, A.D. Chen, C.S. Johnson Jr., J. Magn. Reson. Ser. A 115 (1995) 260.
[26] C.S. Johnson Jr., Prog. Nucl. Magn. Reson. Spectrosc. 34 (1999) 203.
[27] D.Y. Zhao, J.L. Feng, Q.S. Huo, N. Melosh, G.H. Fredrickson, B.F. Chmelka, G.D. Stucky, Science 279 (1998) 548.
[28] D. Müller, W. Gessner, H.J. Behrens, G. Scheler, Chem. Phys. Lett. 79 (1981) 59.
[29] G.M. Loudon, Organic Chemistry, Benjamin/Cummings, Menlo Park, CA, 1988.
[30] C. Perego, S. Amarilli, R. Millini, G. Bellussi, G. Girotti, G. Terzoni, Micropor. Mater. 6 (1996) 395.
[31] A.B. Deshpande, A.R. Bajpai, S.D. Samant, Appl. Catal. A 209 (2001) 229.
[32] H.S. Fogler, Elements of Chemical Reaction Engineering, Prentice–Hall, Englewood Cliffs, NJ, 1992.
[33] J. Kärger, D.M. Ruthven, Diffusion in Zeolites and Other Microporous Solids, Wiley, New York, 1992.
[34] R. Roque-Malherbe, R. Wendelbo, A. Mifsud, A. Corma, J. Phys. Chem. 99 (1995) 14064.
[35] S.M. Auerbach, J. Chem. Phys. 106 (1997) 7810.
[36] F. Stallmach, A. Graser, J. Kärger, C. Krause, M. Jeschke, U. Oberhagemann, S. Spange, Micropor. Mesopor. Mater. 44 (2001) 745.
[37] R. Aris, Introduction to the Analysis of Chemical Reactors, Prentice–Hall, Englewood Cliffs, NJ, 1965.
[38] J. Čejka, B. Wichterlová, Catal. Rev. 44 (2002) 375.
[39] S. Bhatia, J. Beltramini, D.D. Do, Catal. Rev.-Sci. Eng. 31 (1989) 431.
[40] P.C. Mihindou-Koumba, H.S. Cerqueira, P. Magnoux, M. Guisnet, Ind. Eng. Chem. Res. 40 (2001) 1042.